Journal of Materials Chemistry C

Thermally stable and strongly emitted CPL in Eu(*D*-facam)$_3$ hybrid solid with alkylammonium salt.

Journal:	*Journal of Materials Chemistry C*
Manuscript ID	TC-ART-11-2022-004670.R1
Article Type:	Paper
Date Submitted by the Author:	23-Nov-2022
Complete List of Authors:	Li, Ziying; Chiba University, Nakamura, Kazuki; Graduate School of Advanced Integration Science, Chiba University, Department of Image and Materials Science Kobayashi, Norihisa; Graduate School of Advanced Integration Science, Chiba University, Department of Image and Materials Science

ARTICLE

Thermally stable and strongly emitted CPL in Eu(*D*-facam)$_3$ hybrid solid with alkylammonium salt

Received 00th January 20xx,
Accepted 00th January 20xx

DOI: 10.1039/x0xx00000x

Ziying Li, Kazuki Nakamura, Norihisa Kobayashi*

A novel europium-based hybrid material, Eu(*D*-facam)$_3$-TMAOAc (tetramethylammonium acetate), with ultra-high luminescence, excellent circular polarization and remarkable thermostability was prepared. Its photophysical performance was studied based on the luminescence properties and energy transfer process. Compared to Eu(*D*-facam)$_3$, Eu(*D*-facam)$_3$-TMAOAc exhibited much brighter luminescence and stronger circular polarization. Additionally, Eu(*D*-facam)$_3$-TMAOAc well retained its structure and luminescence properties even after a heat treatment of 200 °C for 24 hours, whereas Eu(*D*-facam)$_3$ rapidly decomposed. The characteristics of Eu(*D*-facam)$_3$-TMAOAc was characterized by TG analysis, elemental analysis, ESI-mass, PXRD, and FT-IR spectroscopy. It was found that TMAOAc worked as a bidentate bridge linking with Eu(*D*-facam)$_3$ at a 1:1 ratio. This coordination structure contributed to the excellent photophysical properties and thermal stability of Eu(*D*-facam)$_3$-TMAOAc. Furthermore, Eu(*D*-facam)$_3$-TMAOAc showed a high solubility in common organic solvents, and it could keep its outstanding luminescence properties in solid as well as solution states.

Introduction

Trivalent lanthanide complexes have attracted considerable attention owing to their characterized luminescence properties including sharp and abundant emission lines, long emission lifetime, and large pseudo-Stokes shifts for high transparency in the visible light range. They are promising materials in widespread applications such as bio-probing, bio-sensing[1–6] and electroluminescent devices.[7–10] These complexes are also expected as potential circularly polarized luminescence (CPL) luminophores. CPL spectroscopy measures the differential emission intensity of the right and left circularly polarized light, and thus reflects the excited state of chiral luminophores.[11] At a certain particular emission wavelength, the dissymmetry factor of CPL (g_{lum}) is defined as $2(I_L - I_R)/(I_L + I_R)$ where I_L (I_R) is the intensity of the left (right) circularly polarized luminescence. Chiral lanthanide complexes are potential candidates for CPL luminophores because it shows high values of g_{lum}, two orders of magnitude greater than those observed in organic luminophores.[11] The interest in CPL has significantly increased with the development of high-sensitive bioassays[12,13] and high-resolution 3D displays[9,14,15]. Despite most of those applications preferring solid-state luminophores with high CPL activities, there are few solid-state complexes with reported CPL.[16,17] (S1.) In addition, materials with both high luminescence and circular polarization are rarely reported even in the solution state. Moreover, the poor thermal stability of lanthanide complexes also significantly limits their practical applications.[18,19] The preparation of a highly luminescent material with effective CPL as well as outstanding thermostability is therefore of primary importance.

In recent decades, hybrid lanthanide materials such as coordination polymers[20,21], metal–organic frameworks,[22,23,24] and nanocomposites,[25,26] have become the focus of considerable research interest. This is because the lanthanide-based hybrid materials have a better emission output and thermal stability than the single lanthanide complexes owing to their hybridization structures.[18] In these lanthanide hybrid systems, carboxylate compounds are widely used as a linkage between lanthanide ions, [5,18,21,22] because lanthanide ions are hard Lewis acids and prone to interact with hard anions such as carbonate and carboxylate ions.[27]

In our previous study, the outstanding luminescence performance of the Eu(III) complex (Eu(*D*-facam)$_3$) was observed in the presence of tetramethylammonium acetate (TMAOAc) in alcohol.[28,29] It was found that the interaction between Eu(*D*-facam)$_3$ and TMAOAc contributed to a significant improvement in luminescence properties of Eu(*D*-facam)$_3$ in solution. However, solid system towards device fabrication and practical application of this excellent circularly polarized luminescent Eu(III) material was not investigated yet. In this study, a new Eu(III) hybrid material, Eu(*D*-facam)$_3$-TMAOAc, was successfully obtained in a solid state from Eu(*D*-facam)$_3$/ TMAOAc mixed solutions. It was revealed that TMAOAc acted as a bidentate bridge with a function of linking Eu^{3+} ions leading to a chain structure similar to coordination polymers. The photophysical properties, thermal behaviours, and

[a] *Graduate School of Engineering, Chiba University, 1-33 Yayoi-cho, Inage-ku, Chiba, 263-8522, Japan. E-mail: koban@faculty.chiba-u.jp.*

† Footnotes relating to the title and/or authors should appear here.

Electronic Supplementary Information (ESI) available: [details of any supplementary information available should be included here]. See DOI: 10.1039/x0xx00000x

coordination structures of Eu(*D*-facam)$_3$-TMAOAc were investigated in detail. This Eu(III) hybrid material exhibited outstanding luminescence properties, remarkable superiority in CPL activity and thermal stability in the solid state, showing its considerable potential for practical CPL applications.

Experimental section

Materials

All chemicals were commercially available and were used as received. Europium tris[3-(trifluoromethylhydroxymethylene)-(+)-camphorate] (Eu(*D*-facam)$_3$) and tetramethylammonium acetate (TMAOAc) was purchased from Sigma-Aldrich, Japan. The solvents, 1-butanol, acetone, were purchased from Tokyo Chemical Industry Co. Ltd., Japan.

Measurement and characterization

Oxygen dissolved in the Eu(III)$_3$ compounds solution was removed by bubbling nitrogen gas through the solution prior to carrying out the optical measurements. The absorption and reflectance spectra were acquired using a UV-visible/NIR spectrophotometer (V-770, JASCO Corporation, Japan). The absorption and circular dichroism (CD) spectra of Eu(*D*-facam)$_3$-TMAOAc solutions were acquired using a circular dichroism spectrometer (J-1100, JASCO Corporation, Japan). The photoluminescence spectra were acquired using a spectrofluorometer (FP-6800, JASCO Corporation, Japan). The circularly polarized luminescence (CPL) measurements were conducted using a previously reported system.[30] This system consists of the following components: a 375 nm LED (M365L2, Thorlabs Japan Inc., Japan), an LED driver (DC2100, Thorlabs Japan Inc., Japan), a photoelastic modulator (PEM-90, Hinds Instruments Inc., United States), a photomultiplier tube (H7732-10, Hamamatsu Photonics K. K., Japan), a linearly polarized cubic prism (200,000 : 1), a photomultiplier tube (H7732-10, Hamamatsu Photonics K. K., Japan), and a dual-phase DSP (digital signal processing) lock-in amplifier (7265, Signal Recovery Ltd., United Kingdom). The appropriate detection wavelengths of the monochromator and the PEM (photoelastic modulator) were controlled using a PC (Dell D11M). Thermogravimetric analysis (TG) spectra were acquired using a thermogravimetry/differential thermal Analyzer (TG/DTA6300, Seiko Instruments Inc., Japan). Elemental analysis was acquired using CHN/O/S elemental analyzer (CE-440F, Exeter Analytical, Inc., United States). Electrospray ionization (ESI) mass spectra were acquired by a hybrid ion trap mass spectrometer (LTQ Orbital XL, Thermo Fisher Scientific, United States). Fourier-transform infrared (FT-IR) spectra were obtained using a FT-IR Spectrometer (FT/IR 680, JASCO Corporation, Japan). Powder diffraction (PXRD) spectra were acquired using a powder X-ray diffractometer (D8 ADVANCE, Bruker AXS, United States).

Preparation of Eu(*D*-facam)$_3$-TMAOAc

A solution of Eu(*D*-facam)$_3$ (89.37 mg, 0.1 mmol) in 1-butanol (10 ml, 10mmol/L) was added to a solution of TMAOAc (66.60 mg, 0.5 mmol) in 1-butanol (10 ml, 50mmol/L). Eu(*D*-facam)$_3$ is a yellow powder, and its high concentration (>5mmol/L) 1-butanol solution shows a pale-yellow colour. By addition of TMAOAc solution, the yellow in Eu(*D*-facam)$_3$ solution quickly disappeared and turned into transparent. White precipitation was observed in transparent mixed solution only within 1 h after mixing. The mixture solution without stirring was set aside for 48h, the white precipitate was filtered, thoroughly washed with deionized water, and allowed to vacuo dry.

Results and discussion

Luminescence performance of Eu(*D*-facam)$_3$-TMAOAc

The absorption spectra of Eu(*D*-facam)$_3$ and the Eu(*D*-facam)$_3$/TMAOAc mixed solution were measured, they are shown in Fig. 1. The concentration of Eu(*D*-facam)$_3$ was fixed at 0.5mmol/L for fair comparison. The absorbance peaks at approximately 300nm were from π–π* transition of ligands and didn't be affected by adding TMAOAc. At high concentration (10 mmol/L) of Eu(III) compounds, colour change of solution was directly observed in the addition of TMAOAc. As shown in Fig. 1 inset, a tiny peak in both solutions at 465 nm was derived from $^5D_2 \leftarrow {}^7F_0$ transition.[31] A broad band of Eu(*D*-facam)$_3$ solution appeared around 400 nm~ owing to the observed yellow colour. On the other hand, lower absorption band in the Eu(*D*-facam)$_3$/TMAOAc mixed solution was observed at the same wavelength, indicating the solution was colourless and transparent. The colour bleaching that occurred in solution suggested a rapid interaction between Eu(*D*-facam)$_3$ and TMAOAc in 1-butanol. The alteration of colour in both solution and solid systems confirmed the successful fabrication of the new Eu(III) hybrid material, Eu(*D*-facam)$_3$-TMAOAc.

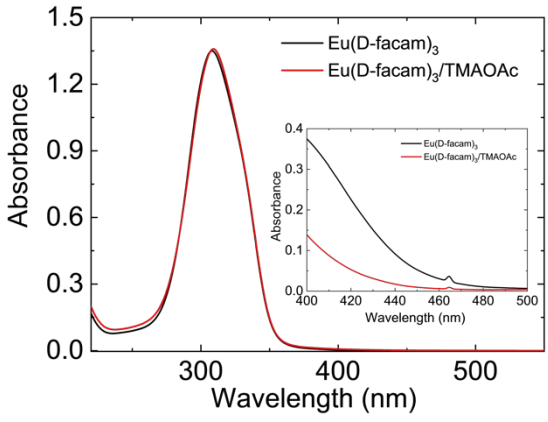

Fig. 1 Absorption spectra of Eu(*D*-facam)$_3$ and the Eu(*D*-facam)$_3$ / TMAOAc mixed solution in 1-butanol. The concentration was fixed to 0.5mmol/L and 10mmol/L(inset).

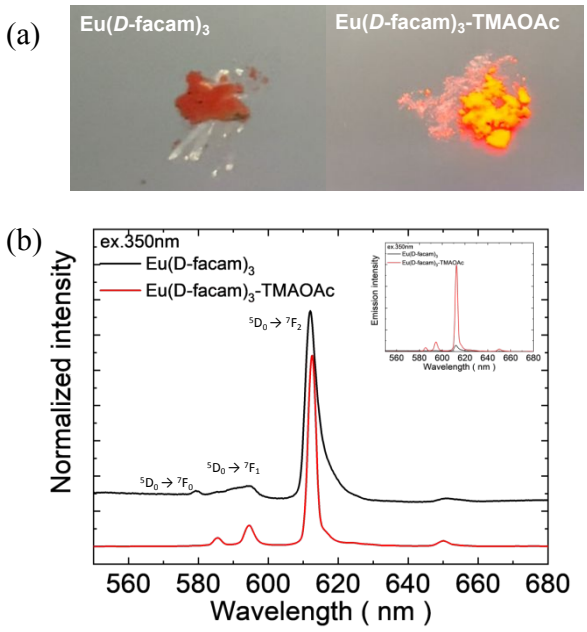

Fig. 2 (a) Digital photographs of luminescent Eu(*D*-facam)$_3$ (left) and Eu(*D*-facam)$_3$-TMAOAc(right) upon irradiation by the UV light (λ = 365 nm). (b)Normalized and original(inset) emission spectra of Eu(*D*-facam)$_3$ and Eu(*D*-facam)$_3$-TMAOAc in solid state. The excitation wavelength was 350 nm.

Fig. 2(a) shows digital photographs of Eu(*D*-facam)$_3$ and Eu(*D*-facam)$_3$-TMAOAc upon irradiation with the UV lamp (λ = 365 nm). Clearly, Eu(*D*-facam)$_3$-TMAOAc exhibited a much stronger red luminescence than Eu(*D*-facam)$_3$. In order to characterize the luminescence properties of Eu(*D*-facam)$_3$-TMAOAc, normalized emission spectra of Eu(*D*-facam)$_3$ and Eu(*D*-facam)$_3$-TMAOAc in the solid state were obtained (Fig. 2(b)). The original emission spectra (inset in Fig. 2(b)) of Eu(*D*-facam)$_3$-TMAOAc exhibited a dramatic increment compared to Eu(*D*-facam)$_3$ which is in agreement with the visually observed luminescence in Fig. 2(a). The characteristic bands of Eu(III) complex corresponding to the $^5D_0 \rightarrow {}^7F_J$ (J = 0–3) transitions are observed at approximately 575, 595, 612 and 650 nm. $^5D_0 \rightarrow {}^7F_0$ transition was reported as an indicator for Eu(III) complexes in specific symmetry systems.[32,33,34] The emission peak derived from $^5D_0 \rightarrow {}^7F_0$ transition in Eu(*D*-facam)$_3$ cannot be observed when Eu(*D*-facam)$_3$ coordinated with TMAOAc, indicating that Eu(*D*-facam)$_3$-TMAOAc has a different symmetry structure from Eu(*D*-facam)$_3$. $^5D_0 \rightarrow {}^7F_1$ is a magnetic dipole (MD) transition, and its radiative rate is independent in the environment around Eu^{3+} ion, and the shape of the emission band directly reflects the crystal-field splitting of the $^7F_1$ level.[31] An obvious split of the emission peak related to the $^5D_0 \rightarrow {}^7F_1$ transitions in Eu(*D*-facam)$_3$-TMAOAc was observed, suggesting that TMAOAc perturbed the crystal fields of Eu(III) complexes. In addition, $^5D_0 \rightarrow {}^7F_2$ transitions are known to be typical electric dipole (ED) transitions that are highly sensitive to the environment around Eu^{3+} ion and the nature of ligands. The dominated emission peaks derived from $^5D_0 \rightarrow {}^7F_2$ transitions became narrower and sharper in Eu(*D*-facam)$_3$-TMAOAc than in Eu(*D*-facam)$_3$, accounting for the changed coordination structure of Eu(III) complexes by interactions with TMAOAc. According to the Judd–Ofelt theory, the hypersensitive $^5D_0 \rightarrow {}^7F_2$ transition is strictly forbidden for Eu^{3+} ion with a centre of symmetry, and, thus, a low-site symmetry around Eu^{3+} ion typically exhibits a more intense emission peak derived from $^5D_0 \rightarrow {}^7F_2$ transition.[31] Moreover, the emission intensity from the $^5D_0 \rightarrow {}^7F_1$ transition is a constant in the total integrated intensity and normally it is used as an 'internal reference'.[35,36] The site symmetry can thus be evaluated by the intensity ratio (I_{rel}) of the integrated intensities from $^5D_0 \rightarrow {}^7F_2$ to $^5D_0 \rightarrow {}^7F_1$ transition.[31] The values of I_{rel} for Eu(*D*-facam)$_3$ and Eu(*D*-facam)$_3$-TMAOAc were calculated to be 10.58 and 6.88, respectively, implying that the interaction between the Eu(III) complex and TMAOAc contributed to a higher site symmetry around Eu^{3+} ion in this new Eu(III) hybrid material. These changes in emission spectra could be attributed to the rearrangement of the coordination geometry in Eu(III) complexes.

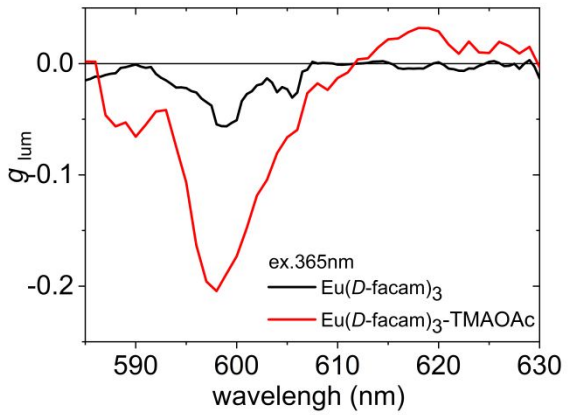

Fig. 3 g_{lum} spectra of Eu(*D*-facam)$_3$ and Eu(*D*-facam)$_3$-TMAOAc in KBr pellet. The excitation wavelength was 365 nm.

The circularly polarized luminescence (CPL) of Eu(III) complexes is largely influenced by their coordination geometries. CPL measurements of Eu(*D*-facam)$_3$ and Eu(*D*-facam)$_3$-TMAOAc were performed in a solid state (in KBr pellets). The dissymmetry factor, g_{lum}, was used to quantitatively evaluate the CPL activity of both Eu(III) compounds in Fig. 3. The value of g_{lum} was calculated by $2(I_L - I_R)/(I_L + I_R)$, and the I_L (I_R) is the intensity of the left (right) circularly polarized luminescence. Therefore, g_{lum} can be used to evaluate the emission ratio of left or right CPL. Characteristic CPL signals were observed at approximately 585–605 and 610–620 nm, corresponding to the emissions from $^5D_0 \rightarrow {}^7F_1$ and $^5D_0 \rightarrow {}^7F_2$ transition, respectively. For $^5D_0 \rightarrow {}^7F_1$ MD transition, a high g_{lum} of -0.21 from Eu(*D*-facam)$_3$-TMAOAc was observed, which was more than four times higher than that of Eu(*D*-facam)$_3$ (g_{lum} = -0.05). The CPL properties of Eu(*D*-facam)$_3$ in the KBr pellet, as observed in this study, agreed well with previous reports.[17] For the $^5D_0 \rightarrow {}^7F_2$ electric transition, a CPL signal of Eu(*D*-facam)$_3$-TMAOAc (g_{lum} = +0.03) was induced, whereas no CPL

was observed in Eu(*D*-facam)$_3$ (g_{lum} = 0). In this novel Eu(III) hybrid material, the right CPL from the $^5D_0 \rightarrow {}^7F_1$ transition was obviously enhanced (g_{lum} = -0.05→-0.21) and left CPL from the $^5D_0 \rightarrow {}^7F_2$ transition was induced (g_{lum} = 0→-0.03). The excellent CPL activity indicated that the chirality environment and coordination structure of Eu(*D*-facam)$_3$ were obviously affected because of the interaction with TMAOAc.

Furthermore, the differential absorbance intensity of the light and left circularly polarized light was measured by circular dichroism (CD) spectroscopy. CD is typically used to investigate the chirality structure of materials as a complementary tool to CPL. The absorption and CD spectra of Eu(*D*-facam)$_3$ and Eu(*D*-facam)$_3$-TMAOAc were then studied in the KBr pellet (Fig. S2). Reproducibility of the CD signal from the film samples was validated by rotating the samples to avoid the artefacts. For both Eu(III) complexes, a broad absorbance band covering 300–350 nm, attributed to π–π* transition from β-diketonate ligands, was observed. In the CD measurement, Eu(*D*-facam)$_3$ did not exhibit any significant peaks and the lack of CD is probably responsible for a weak CPL signal.[37] An obvious positive CD peak at approximately 350 nm was observed in Eu(*D*-facam)$_3$-TMAOAc, indicating the changed spatial disposition of multi-chromophores of β-diketonate ligands. This change was probably ascribed to the interaction with TMAOAc, which presumably could distort the geometric structure of ligands in this Eu(III) hybrid material. The finding in chiroptical properties (CD and CPL) revealed that the interaction between Eu(*D*-facam)$_3$ and TMAOAc shown profound effects on the chirality of β-diketonate ligands and coordination geometry of Eu(III) complexes. These structural change could probably cause the altered electronic structure of Eu(III) complexes owing to the TMAOAc hybridization, which can also be reflected by the affected diffuse reflectance spectra of Eu(III) complexes.

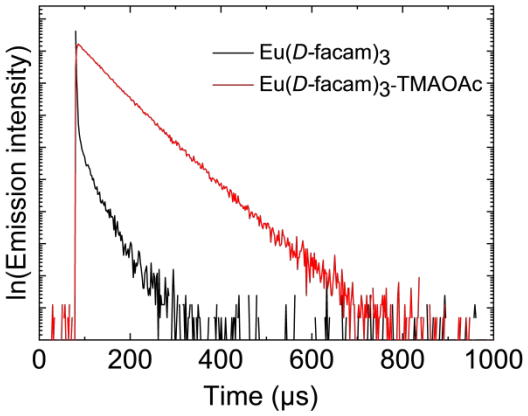

Fig. 4 Emission decay profiles of Eu(*D*-facam)$_3$ and Eu(*D*-facam)$_3$-TMAOAc in solid state. The excitation wavelength was 350 nm.

Tab. 1 Luminescence lifetimes (τ), intrinsic quantum yields (Φ_{Ln}), total quantum yields (Φ_{tot}), efficiencies of sensitization (η_{sens}), radiative rates (k_r), non-radiative rates (k_{nr}), and emission intensity ratios of total to the ED moments (I_{tot}/I_{MD}) for Eu(*D*-facam)$_3$ and Eu(*D*-facam)$_3$-TMAOAc in solid state.

	I_{tot}/I_{MD}	τ (μs)	Φ_{tot} (%)	Φ_{Ln} (%)	k_r (s^{-1})	k_{nr} (s^{-1})	η_{sens} (%)
Eu(*D*-facam)$_3$	11.9	278.5	1.6	16.4	588.4	3002.3	9.7%
Eu(D-facam)$_3$-TMAOAc	7.7	692.1	21.5	26.3	380.7	1064.2	81.6%

In accordance with absorption spectra, diffuse reflectance spectra of both Eu(*D*-facam)$_3$ and Eu(*D*-facam)$_3$-TMAOAc in the solid state also exhibited broad peaks at approximately 350 nm from β-diketonate ligands (Fig. S3). The variation in the shape of both Eu(III) compounds was observed, suggesting that TMAOAc affected the electrical transition of ligands in this new Eu(III) hybrid material.

Eu(*D*-facam)$_3$-TMAOAc presented much better luminescence performance than Eu(*D*-facam)$_3$ even in the condition of a higher symmetry. Higher symmetry around Eu^{3+} contributed to a low radiative rate constant, leading to a low emission intensity.[38] To further elucidate the photophysical properties of Eu(III) complexes, their energy transfer process was precisely analysed. Firstly, the time-resolved emission profiles (Fig. 4) and the quantum yield of Eu(*D*-facam)$_3$ and Eu(*D*-facam)$_3$-TMAOAc in the solid state were measured (Tab. 1). The values of lifetime (τ) and quantum yield (Φ_{tot}) for Eu(*D*-facam)$_3$ was 278.5 μs and 1.6%, respectively. A significant enhancement was obtained in Eu(*D*-facam)$_3$-TMAOAc with 692.1 μs and 21.5% for τ and Φ_{tot}, respectively, which was consistent with the photographs of the bright luminescence from Eu(*D*-facam)$_3$-TMAOAc as seen in Fig. 1(a).

A series of key photophysical parameters were estimated and the values are shown in Tab. 1. The radiative rate constant (k_r) and non-radiative rate constant (k_{nr}) were calculated as follows:

$$k_r = A_{MD,0} \times n^3 \times \left(\frac{I_{tot}}{I_{MD}}\right)$$

$$\tau = \frac{1}{k_r + k_{nr}}, \quad k_{nr} = \frac{1}{\tau} - k_r$$

where $A_{MD,0}$ is the spontaneous emission probability for the $^5D_0 \rightarrow {}^7F_1$ magnetic dipole transition in vacuo (14.65 s^{-1}), n is the refractive index of the medium (1.5 for solid) and I_{tot}/I_{MD} is the ratio of total integrated area of emission spectrum to the area of the $^5D_0 \rightarrow {}^7F_1$ band.

The intrinsic quantum yield (Φ_{Ln}) and sensitization efficiency of the lanthanide luminescence by the ligands (η_{sens}) was then evaluated by:

$$\Phi_{Ln} = \frac{k_r}{k_r + k_{nr}}, \quad \eta_{sens} = \frac{\Phi_{tot}}{\Phi_{Ln}}$$

Compared to Eu(*D*-facam)$_3$, a decrease in the radiative rate constant for Eu(*D*-facam)$_3$-TMAOAc was observed, corresponding to its higher symmetry. This is because, in the Eu(III) complex with higher symmetry, the forbidden electric dipole transitions in the Judd-Ofelt theory would be more strictly forbidden and thus leading to a lower radiative rate constant.[31] In addition, the non-radiative rate constant for Eu(*D*-facam)$_3$-TMAOAc was significantly suppressed (3002.3 s^{-1} → 1064.2 s^{-1}). In this condition, the competition ability of the radiative process for Eu(*D*-facam)$_3$-TMAOAc is stronger than Eu(*D*-facam)$_3$ in emission pathways, so a higher intrinsic quantum yield in Eu(*D*-facam)$_3$-TMAOAc was obtained. Therefore, the total superior photophysical properties was observed in Eu(*D*-facam)$_3$-TMAOAc even with a higher symmetry. Based on these variations, the sensitization efficiency of Eu(*D*-facam)$_3$-TMAOAc was significantly improved to 81.6%, obviously higher than that of Eu(*D*-facam)$_3$ (9.7%). Compared to an improved sensitization efficiency of 28% in the Eu(*D*-facam)$_3$/TMAOAc mixed solution previously reported,[28] the new Eu(III) hybrid material in this study made a significant progress in the sensitization performance of the original Eu(*D*-facam)$_3$. This was likely because the interaction between Eu(III) complexes and TMAOAc decreases the distance between Eu^{3+} ion and the β-diketonate ligands, and the shorter donor–acceptor distance can accelerate the energy transfer rate for a higher sensitization efficiency.[39]

Thermostability and interaction ratio of Eu(*D*-facam)$_3$-TMAOAc

Lanthanide complexes are typically difficult to maintain a stable structure and luminescence at a high temperature for a long time, although many applications require thermal stability. Therefore, the thermal stability for the luminescence and structure of both Eu(III) compounds was investigated after a long-time heat treatment and cooling to room temperature. Emission spectra (Fig. S4) and emission decay profiles of Eu(*D*-facam)$_3$ and Eu(*D*-facam)$_3$-TMAOAc were obtained at room temperature before and after the heat treatment of 150 °C for 24 h. The emission peaks of both Eu(III) compounds were not changed, suggesting their stable coordination structures after 150 °C heat treatment. In addition, the decrease of the emission lifetime was 9.8% for Eu(*D*-facam)$_3$ and 0.8% for Eu(*D*-facam)$_3$-TMAOAc. Therefore, both Eu(III) compounds maintained their luminescence performance after the 150 °C heat-treatment. On the other hand, a notable difference in the physical state and luminescence performance between Eu(*D*-facam)$_3$ and Eu(*D*-facam)$_3$-TMAOAc were observed upon heat treatment at 200 °C for 24 h. Eu(*D*-facam)$_3$ quickly melted and turned into a dark adhesive through heating at 200 °C. This could be explained by the fact that Eu(*D*-facam)$_3$ lost its complex structure and luminescence, which was invisible to the naked eye, upon UV irradiation (Fig. S5(a)). In contrast, Eu(*D*-facam)$_3$-TMAOAc well maintained its solid state and bright luminescence even after 24 h of the heat treatment at 200 °C (Fig. S5(b)). As seen in Tab. 2, the emission lifetime of melted Eu(*D*-facam)$_3$ and well state-maintained Eu(*D*-facam)$_3$- TMAOAc was 42.3 μs and 682.9 μs, respectively. Eu(*D*-facam)$_3$-TMAOAc kept its high luminescence properties with a slight loss of 1.3% in the emission

Tab. 2 Luminescence lifetimes for Eu(*D*-facam)$_3$ and Eu(*D*-facam)$_3$-TMAOAc before and after 24 hours heat-treatment of 150 °C and 200 °C in solid state.

	τ (μs) before heat-treatment	τ (μs) after heat-treatment for 24 hours	
		150°C	200°C
Eu(*D*-facam)$_3$	278.5	251.2	42.3
Eu(*D*-facam)$_3$-TMAOAc	692.1	686.6	682.9

lifetime, whereas Eu(*D*-facam)$_3$ reduced the lifetime by 84.8%. Fourier-transform infrared spectra (FT-IR) of Eu(*D*-facam)$_3$-TMAOAc before and after 24 h of the heat treatment at 200 °C were obtained (Fig. S6). There is no change in FT-IR before and after heat treatment, confirming the high thermal stability of the structure and physical state of Eu(*D*-facam)$_3$-TMAOAc, consistent with above results. Acutually, TMAOAc itself was very unstable at high temperatures above 150 °C. The improved thermal stability for both Eu(*D*-facam)$_3$ and TMAOAc in this new hybrid material could be ascribed to their stable interactions.

Furthermore, the red luminescence of Eu(*D*-facam)$_3$-TMAOAc was maintained even at high temperatures. As shown in Fig. 5(a), sharp and intense emission peaks of Eu(*D*-facam)$_3$-TMAOAc were observed even at 100 °C. The shape of emission peaks was consistent with those obtained by the room-temperature measurements, suggesting the stable luminescence properties and coordination structure of Eu(*D*-facam)$_3$-TMAOAc at 100 °C. On the contrary, the luminescence of Eu(*D*-facam)$_3$ was totally quenched with no emission peaks at 100 °C (Fig. 5(b)). During the energy transfer process of Eu(III) complexes, the radiative rate constant (k_r) is independent of the temperature, and the non-radiative rate constant (k_{nr}) is known as a temperature-dependent parameter.[40] The intrinsic quantum yield (Φ_{Ln}) can be calculated as $k_r/(k_r+k_{nr})$. In the case of Eu(*D*-facam)$_3$, the enhanced k_{nr} at 100 °C gave rise to a significant increase in the denominator, making Φ_{Ln} extremely close to zero. The luminescence of Eu(*D*-facam)$_3$ at 100 °C was thus extinguished. Conversely, Eu(*D*-facam)$_3$-TMAOAc exhibited a much lower k_{nr} (1064.2 s^{-1} at room temperature) than Eu(*D*-facam)$_3$ (3002.3 s^{-1} at room temperature), so the denominator, (k_r+k_{nr}), at 100 °C for Eu(*D*-facam)$_3$-TMAOAc was much smaller than that for Eu(*D*-facam)$_3$. Therefore, Φ_{Ln} of Eu(*D*-facam)$_3$-TMAOAc at 100 °C maintained a relatively substantial value, accounting for the red luminescence even at a high temperature.

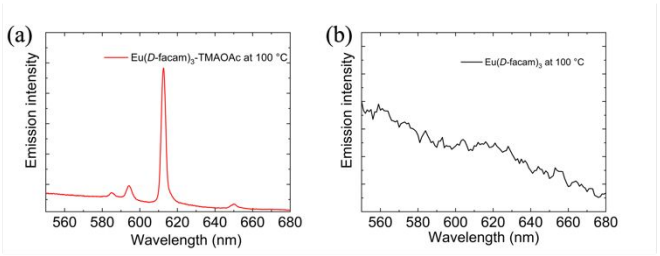

Fig. 5 Emission spectra of (a) Eu(*D*-facam)$_3$-TMAOAc and (b) Eu(*D*-facam)$_3$ at 100°C in solid state.

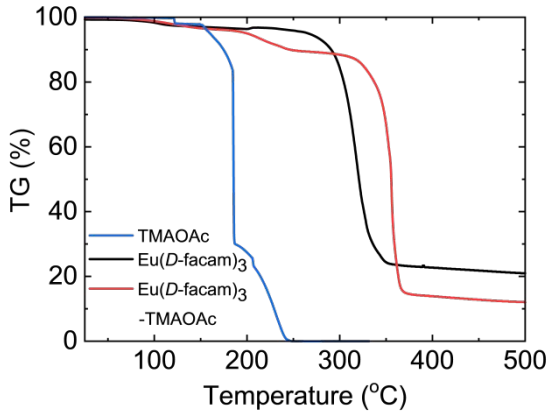

Fig. 6 TG analysis of Eu(*D*-facam)$_3$, TMAOAc and Eu(*D*-facam)$_3$-TMAOAc.

The thermal properties of Eu(*D*-facam)$_3$-TMAOAc were investigated by thermogravimetric (TG) analysis. Fig. 6 shows the weight-loss process of Eu(*D*-facam)$_3$, TMAOAc, and Eu(*D*-facam)$_3$-TMAOAc at 20–500 °C. Eu(*D*-facam)$_3$-TMAOAc showed improved thermal stability up to 320 °C, whereas a successive mass loss of Eu(*D*-facam)$_3$ started at 270 °C. In the case of TMAOAc, two decomposition steps were observed for TMA^+ and OAc^-, respectively. The complete thermal decomposition of TMAOAc occurred at 250 °C, accompanied by a mass loss of 100%. Interestingly, Eu(*D*-facam)$_3$-TMAOAc could still exhibit a brilliant luminescence after 24 h of the heat treatment at 250 °C. The excellent thermal stability was ascribed to the stable structure owing to the interaction between Eu(*D*-facam)$_3$ and TMAOAc.

To investigate the interaction ratio of Eu(*D*-facam)$_3$ to TMAOAc in this new hybrid Eu(III) material, elemental analysis (for C, H, and N) was conducted. The calculated and experimental elemental compositions are shown in Tab. 3. The calculated values based on the interaction ratio of 1:1 matched well with the experimental values, and thereby the interaction ratio of Eu(*D*-facam)$_3$ to TMAOAc was estimated to be 1:1.

Moreover, Eu(*D*-facam)$_3$-TMAOAc, precipitated from 1-butanol with high concentrations of both starting materials, is soluble in 1-butanol at a relatively low concentration (0.2 mmol/L). Based on our previous report, a higher concentration of TMAOAc could lead to the site symmetry around Eu^{3+} ion being increased (decreased I_{rel}) and emission peaks changed.[28] The emission spectra of Eu(*D*-facam)$_3$-TMAOAc and a mixed solution of Eu(*D*-facam)$_3$ and TMAOAc with a concentration ratio of 1:1 in 1-butanol were measured (Fig. S7). The

Tab. 3 Elemental analysis of Eu(*D*-facam)$_3$-TMAOAc.

C (%)		H (%)		N (%)	
calcd.	found	calcd.	found	calcd.	found
49.13	49.50	5.60	5.59	1.36	1.33

Tab. 4 Results of TG-DTA analysis of Eu(*D*-facam)$_3$-TMAOAc.

Temperature range (°C)	Mass loss (%) found (calcd.)	Probable lost molecules	Residue mass (%) found(calcd.)	Composition of the residue
100∽320	12.90 (12.89)	TMAOAc		
320∽370	72.48 (72.35)	*D*-facam	14.62(14.76)	Eu_2O_3

perfectly matched emission spectra and the same site symmetry (I_{rel} = 6.45) indicated that their identical coordination structures still maintained even in solution state, further supporting the 1:1 interaction ratio between TMAOAc and Eu(*D*-facam)$_3$ in Eu(*D*-facam)$_3$-TMAOAc.

Based on the confirmed interaction ratio, the experimental and corresponding theoretical thermoanalytical data of Eu(*D*-facam)$_3$-TMAOAc are shown in Tab. 4. The first mass loss stage in Eu(*D*-facam)$_3$-TMAOAc was observed from 100 to 320 °C, which was a gradual mass loss, likely, from TMAOAc. The total loss during the first stage was 12.90%, which was close to the calculated loss percentage (12.89%), further verifying the 1:1 interaction ratio between Eu(*D*-facam)$_3$ and TMAOAc. The second main successive mass loss stage was from 320 to 370 °C, and the corresponding mass loss of 72.48% was attributed to the loss of (*D*-facam) ligands. The final residue was predicted as Eu_2O_3, which was also consistent with the theoretical value. In addition, one thermal decomposition step of the ligands loss in Eu(*D*-facam)$_3$ occurred at 270 °C. Therefore, Eu(*D*-facam)$_3$-TMAOAc exhibited better thermal stability than Eu(*D*-facam)$_3$. The interaction between Eu(*D*-facam)$_3$ and TMAOAc at 1:1 ratio significantly contributed to both the outstanding luminescence performance and thermal stability in Eu(*D*-facam)$_3$-TMAOAc.

Structure analysis of Eu(*D*-facam)$_3$-TMAOAc

To elucidate the impressive improvement in optical behaviours and thermal stability of this Eu(III) hybrid material, the structures and configurations were studied. Electrospray ionization (ESI) mass spectroscopy of Eu(*D*-facam)$_3$-TMAOAc was firstly conducted. A series of experimental and corresponding calculated mass signals identifying the coordination structure of this Eu(III) hybrid material was obtained. All the experimental mass spectra were highly consistent with the calculated signals, ensuring the reliability of the following fragments. The fragments of $[Eu(D\text{-facam})_3{\cdot}TMA]^+$, $[Eu(D\text{-facam})_3{\cdot}OAc]^-$, $[Eu(D\text{-facam})_3{\cdot}TMA{\cdot}2OAc]^-$, and $[Eu(D\text{-facam})_3{\cdot}2TMA{\cdot}OAc]^+$ (Fig. S8) indicated the interaction between the single Eu(*D*-facam)$_3$ and TMAOAc. $[2Eu(D\text{-facam})_3{\cdot}TMA]^+$, $[2Eu(D\text{-facam})_3{\cdot}OAc]^-$, $[2Eu(D\text{-facam})_3{\cdot}TMA{\cdot}2OAc]^-$, and $[2Eu(D\text{-facam})_3{\cdot}2TMA{\cdot}OAc]^+$ (Fig. S9) demonstrated that multi-Eu(III) complexes were associated via TMAOAc.

It was reported that acetates could act as a bidentate ligand binding to lanthanide ions.[41] In our study, acetates probably play a similar role as a bidentate bridge to link multiple Eu^{3+} ions and form a chain structure of Eu(III) complexes. As many studies have reported, carboxylate compounds generally act as a linkage to form the

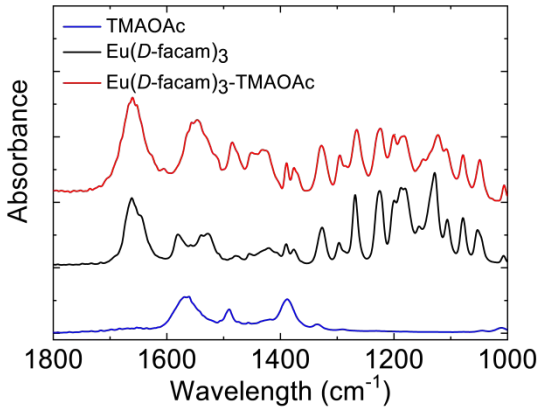

Fig. 7 FT-IR spectra of Eu(*D*-facam)$_3$, TMAOAc and Eu(*D*-facam)$_3$-TMAOAc.

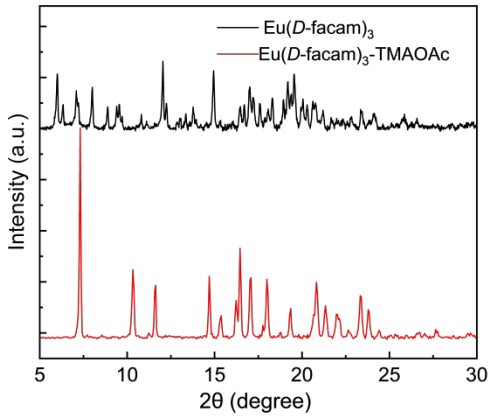

Fig. 8 Powder X-ray diffraction spectra of Eu(*D*-facam)$_3$ and Eu(*D*-facam)$_3$-TMAOAc.

lanthanide polymer with remarkable luminescence and stability.[5,18,21,22] In such chain structure, the distance between a donor and an accepter (ligand-Eu^{3+}) in the Eu(III) hybrid materials is typically shorter than single complex. Therefore, Eu(*D*-facam)$_3$-TMAOAc was endowed with a significant accelerated transfer energy (high sensitization efficiency) and enhanced emission intensity. Moreover, the Eu(III) coordination polymers are known to decrease vibrational quenching because of their chain-structural rigidness.[42] Thus, the non-radiative rate was significantly suppressed (3002.3 s^{-1} → 1064.21 s^{-1}) in Eu(*D*-facam)$_3$-TMAOAc with its rigid chain structures.

In our previous study concerning solution state, the effect of a series of ammonium salts with various cations and anions on Eu(III) complexes was investigated. The results demonstrated the irreplaceability of both TMA^+ and OAc^- in the photoluminescence improvement of Eu(*D*-facam)$_3$. In this study, the fragments were also indicative of the importance of both TMA^+ and OAc^- in this novel Eu(III) hybrid material. TMAOAc was indispensable to improve luminescence properties of Eu(*D*-facam)$_3$ in both solution and solid states.

Fig. 7 shows the FT-IR spectra of Eu(*D*-facam)$_3$, TMAOAc, and Eu(*D*-facam)$_3$-TMAOAc. For Eu(*D*-facam)$_3$, two peaks shown in the range 1500–1600 cm^{-1} suggested the C═C═C stretching vibration of β-diketonate moiety in Eu(*D*-facam)$_3$.[43] The double peaks merged into one peak at around 1550 cm^{-1} in Eu(*D*-facam)$_3$-TMAOAc, indicating the more equivalent C═C═C bonding. In TMAOAc, the peaks at around 1560 and 1390 cm^{-1} were attributed to the antisymmetric and symmetric stretching vibration of COO^-, respectively.[44] With respect to Eu(*D*-facam)$_3$-TMAOAc, the COO^- antisymmetric stretching vibration shifted from 1560 to 1550 cm^{-1}, and signals at around 1420 cm^{-1} were slightly enhanced due to the COO^- symmetric stretching vibration. Nakamoto reported that the difference (delta value) between the COO^- antisymmetric and symmetric stretching frequencies could be used to determine the bonding mode of acetate groups.[45] The ionic mode (TMAOAc itself) and bridging mode (Eu(*D*-facam)$_3$-TMAOAc) both showed delta value of 140–170 cm^{-1}, whereas the unidentate mode had a much larger delta value of 200–300 cm^{-1}. In Eu(*D*-facam)$_3$-TMAOAc, the delta value of 160 cm^{-1} was clear evidence for the bidentate-bridging role of OAc^- and its chain structure.

In terms of the crystallization of the hybrid material, only tiny needle-like crystals were obtained. The powder X-ray diffraction (PXRD) of Eu(*D*-facam)$_3$-TMAOAc was conducted for the structure investigation (Fig. 8). Eu(*D*-facam)$_3$ showed broad and weak signals which were attributed to its low crystalline state. In contrast, sharp and strong signals from Eu(*D*-facam)$_3$-TMAOAc were observed. Although no single crystal for the structure determination was acquired, it verified the high crystallinity of Eu(*D*-facam)$_3$-TMAOAc. From both ESI mass and PXRD measurements, Eu(*D*-facam)$_3$-TMAOAc presumably acted as a chain structure, and the TMAOAc linkage resulted in a change in the coordination geometry of Eu(*D*-facam)$_3$, as reflected by the PXRD signal shift. The preparation of the single crystal of Eu(*D*-facam)$_3$-TMAOAc is still undergoing in various crystallization conditions, and the detailed crystalline structure of this new Eu(III) hybrid material will be presented in the near future.

Solubility of Eu(*D*-facam)$_3$-TMAOAc

Most Eu(III)-based coordination polymer materials typically have a low solubility in organic solvents.[46] However, Eu(*D*-facam)$_3$-TMAOAc presented a decent solubility in most organic solvents, such as acetone, acetonitrile, chloroform, dimethyl sulfoxide and some alcohols.

Interestingly, although acetone, one of the most common organic solvents, does not dissolve TMAOAc itself, the new Eu(III) hybrid material in this study can be easily dissolved in acetone. This suggested that TMAOAc and Eu(*D*-facam)$_3$ was stably interacted in the Eu(*D*-facam)$_3$-TMAOAc. Therefore, acetone is the optimal solvent

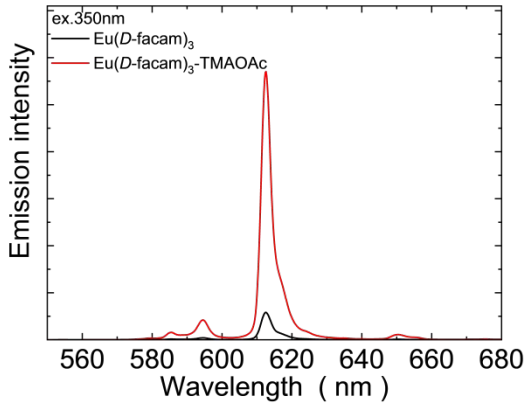

Fig. 9 Emission spectra of Eu(*D*-facam)$_3$ and Eu(*D*-facam)$_3$-TMAOAc in acetone. The excitation wavelength was 350 nm.

for the investigation of the luminescence performance of Eu(*D*-facam)$_3$-TMAOAc in the solution state. Fig. 9 shows the emission spectra of Eu(*D*-facam)$_3$ and Eu(*D*-facam)$_3$-TMAOAc in acetone. Eu(*D*-facam)$_3$-TMAOAc exhibited a stronger emission intensity than that of Eu(*D*-facam)$_3$. Correspondingly, the measured emission lifetime of Eu(*D*-facam)$_3$-TMAOAc (363.0 μs) was longer than that of Eu(*D*-facam)$_3$ (211.3 μs). Therefore, this new Eu(III) hybrid material, Eu(*D*-facam)$_3$-TMAOAc, exhibited outstanding luminescence performance in both solid and solution states.

Conclusions

This study presented a new Eu(III) hybrid material, (Eu(*D*-facam)$_3$-TMAOAc), prepared through a simple synthesis method, which based on the deepening of luminescence improvement in our previous research. Differencing from the earlier solution system, this study mainly targeted a solid system which is more suitable for practical applications. Compared to single complex, Eu(*D*-facam)$_3$-TMAOAc exhibited significant improvements in the luminescence, circular polarization, and thermal stability. This novel Eu(III) hybrid material well maintained its structure and luminescence properties even after 24 h of heat treatment at 200 °C. The enhancement was primarily attributed to its chain structure, in which TMAOAc acted as a bidentate-bridging molecule, linking with Eu(*D*-facam)$_3$ at a 1:1 ratio. In addition, the outstanding luminescence performance of Eu(*D*-facam)$_3$-TMAOAc was obtained in both solid and solution states. This novel Eu(III) hybrid material has considerable potential for applications, such as in CPL luminophores and bioassays.

Conflicts of interest

There are no conflicts to declare.

Acknowledgements

This work was partly supported by JSPS KAKENHI Grant Numbers 17H06377, 20K05641. Z. Li, one of the authors, received financial support from by JST SPRING Grant Number JPMJFS2107 and Initiative for Realizing Diversity in the Research Environment (Japan).

Notes and references

1 W. L. Scaff, D. L. Dyer and K. Mori, *J. Bacteriol.*, 1969, **98**, 246–248.
2 H. Tsukube and S. Shinoda, *Chem. Rev.*, 2002, **102**, 2389–2404.
3 J. Yuan and G. Wang, *J. Fluoresc.*, 2005, **15**, 559–568.
4 S. V. Eliseeva and J.-C. G. Bünzli, *Chem. Soc. Rev.*, 2009, **39**, 189–227.
5 Y. Hasegawa and Y. Kitagawa, *J. Photochem. Photobiol. C Photochem. Rev.*, 2022, **51**, 100485.
6 M. A. Martin, A. I. Olives, B. del Castillo and J. C. Menendez, *Curr. Pharm. Anal.*, **4**, 106–117.
7 M. D. McGehee, T. Bergstedt, C. Zhang, A. P. Saab, M. B. O'Regan, G. C. Bazan, V. I. Srdanov and A. J. Heeger, *Adv. Mater.*, 1999, **11**, 1349–1354.
8 R. C. Evans, P. Douglas and C. J. Winscom, *Coord. Chem. Rev.*, 2006, **250**, 2093–2126.
9 U. Giovanella, M. Pasini, C. Freund, C. Botta, W. Porzio and S. Destri, *J. Phys. Chem. C*, 2009, **113**, 2290–2295.
10 K. Guido, *Hybrid Materials: Synthesis, Characterization, and Applications*, Wiley-VCH Verlag GmbH & Co. KGaA, Germany, 2007.
11 R. Carr, PHD thesis, Durham University, 2014.
12 C. P. Montgomery, B. S. Murray, E. J. New, R. Pal and D. Parker, *Acc. Chem. Res.*, 2009, **42**, 925–937.
13 G. Muller, *Dalton Trans.*, 2009, **44**, 9692–9707.
14 S. M. Jeong, Y. Ohtsuka, N. Y. Ha, Y. Takanishi, K. Ishikawa, H. Takezoe, S. Nishimura and G. Suzaki, *Appl. Phys. Lett.*, 2007, **90**, 211106.
15 D.-W. Zhang, M. Li and C.-F. Chen, *Chem. Soc. Rev.*, 2020, **49**, 1331–1343.
16 F. Zinna and L. Di Bari, *Chirality*, 2015, **27**, 1–13.
17 Y. Kondo, S. Suzuki, M. Watanabe, A. Kaneta, P. Albertini and K. Nagamori, *Front. Chem.*, 2020, **8**, 527.
18 B. Yan, *RSC Adv.*, 2012, **2**, 9304–9324.
19 M. Fernandes, S. S. Nobre, M. C. Gonçalves, A. Charas, J. Morgado, R. A. S. Ferreira, L. D. Carlos and V. de Zea Bermudez, *J Mater Chem*, 2009, **19**, 733–742.
20 Y. Hirai, T. Nakanishi, Y. Kitagawa, K. Fushimi, T. Seki, H. Ito and Y. Hasegawa, *Angew. Chem. Int. Ed.*, 2016, **55**, 12059–12062.
21 S. V. Eliseeva, D. N. Pleshkov, K. A. Lyssenko, L. S. Lepnev, J.-C. G. Bünzli and N. P. Kuzmina, *Inorg. Chem.*, 2010, **49**, 9300–9311.
22 H. Zhang, L. Zhou, J. Wei, Z. Li, P. Lin and S. Du, *J. Mater. Chem.*, 2012, **22**, 3457–3461.
23 J.-C. Rybak, M. Hailmann, P. R. Matthes, A. Zurawski, J. Nitsch, A. Steffen, J. G. Heck, C. Feldmann, S. Götzendörfer, J. Meinhardt, G. Sextl, H. Kohlmann, S. J. Sedlmaier, W. Schnick and K. Müller-Buschbaum, *J. Am. Chem. Soc.*, 2013, **135**, 6896–6902.
24 N.N. Golovnev, M.S. Molokeev, S.N. Vereshchagin and V.V. Atuchin, *J. Coord. Chemistry.*, 2015, **68**, 1865-1877.
25 A. A. Ansari, A. K. Parchur, M. K. Nazeeruddin and M. M. Tavakoli, *Coord. Chem. Rev.*, 2021, **444**, 214040.
26 X. Li, Y. Xie, B. Song, H.-L. Zhang, H. Chen, H. Cai, W. Liu and Y. Tang, *Angew. Chem. Int. Ed.*, 2017, **56**, 2689–2693.
27 M. L. Aulsebrook, B. Graham, M. R. Grace and K. L. Tuck, *Coord. Chem. Rev.*, 2018, **375**, 191–220.

28 Z. Li, H. Minami, K. Nakamura and N. Kobayashi, *ChemPhysChem*, 2021, **22**, 2511–2516.
29 Z. Li, K. Nakamura and N. Kobayashi, *The Imaging Society of Japan,* 2021, **61**, 194–199.
30 H. Tsumatori, T. Nakashima and T. Kawai, *Org. Lett.*, 2010, **12**, 2362–2365.
31 K. Binnemans, *Coord. Chem. Rev.*, 2015, **295**, 1–45.
32 W. C. Nieuwpoort and G. Blasse, *Solid State Commun.*, 1966, **4**, 227–229.
33 V. V. Atuchin, A. S. Aleksandrovsky, O.D. Chimitova, T. A. Gavrilova, A. S. Krylov, M.S. Molokeev, A. S. Oreshonkov, B. G. Bazarov and J. G. Bazarova, *J. Phys. Chem. C.,* 2014, **118**, 15404–15411
34 V.V. Atuchin, A.K. Subanakov, A.S. Aleksandrovsky, B.G. Bazarov, J.G. Bazarova, T.A. Gavrilova, A.S. Krylov, M.S. Molokeev, A.S. Oreshonkov, S.Yu. Stefanovich, *Mater. Des.,* 2018, **40**, 488-494.
35 M. H. V. Werts, R. T. F. Jukes and J. W. Verhoeven, *Phys. Chem. Chem. Phys.*, 2002, **4**, 1542–1548.
36 C. Görller-Walrand, L. Fluyt, A. Ceulemans and W. T. Carnall, *J. Chem. Phys.*, 1991, **95**, 3099–3106.
37 J. P. Riehl and G. Muller, in *Handbook on the Physics and Chemistry of Rare Earths*, ed. K.A. Gschneidner, Jr., J.-C.G. Bünzli and V.K. Pecharsky, Elsevier, Amsterdam, 34, 2004, 220, 289–357.
38 Y. Hasegawa, M. Yamamuro, Y. Wada, N. Kanehisa, Y. Kai and S. Yanagida, *J. Phys. Chem. A*, 2003, **107**, 1697–1702.
39 J. H. S. K. Monteiro, A. de Bettencourt-Dias and F. A. Sigoli, *Inorg. Chem.*, 2017, **56**, 709–712.
40 L. Thompson, J. Legendziewicz, J. Cybinska, L. Pan and W. Brennessel, *J. Alloys Compd.*, 2002, **341**, 312–322.
41 V. L. Garza and N. Purdie, *J. Phys. Chem.*, 1970, **74**, 275–280.
42 K. Miyata, T. Ohba, A. Kobayashi, M. Kato, T. Nakanishi, K. Fushimi and Y. Hasegawa, *ChemPlusChem*, 2012, **77**, 277–280.
43 H. Minami, M. Miyazato, Z. Li, K. Nakamura and N. Kobayashi, *Chem. Commun.*, 2020, **56**, 13532–13535.
44 C. C. R. Sutton, G. da Silva and G. V. Franks, *Chem. – Eur. J.*, 2015, **21**, 6801–6805.
45 K. Nakamoto, *Infrared and Raman Spectra of Inorganic and Coordination Compounds*, John Wiley & Sons, Inc., Hoboken, 1986.
46 G. Calvez, F. Le Natur, C. Daiguebonne, K. Bernot, Y. Suffren and O. Guillou, *Coord. Chem. Rev.*, 2017, **340**, 134–153.